An Effective Approach for Iris Recognition Using Phase-Based Image Matching

Kazuyuki Miyazawa, *Student Member*, *IEEE*, Koichi Ito, *Member*, *IEEE*, Takafumi Aoki, *Member*, *IEEE*, Koji Kobayashi, *Member*, *IEEE*, and Hiroshi Nakajima

Abstract—This paper presents an efficient algorithm for iris recognition using phase-based image matching—an image matching technique using phase components in 2D Discrete Fourier Transforms (DFTs) of given images. Experimental evaluation using the CASIA iris image databases (versions 1.0 and 2.0) and Iris Challenge Evaluation (ICE) 2005 database clearly demonstrates that the use of phase components of iris images makes it possible to achieve highly accurate iris recognition with a simple matching algorithm. This paper also discusses the major implementation issues of our algorithm. In order to reduce the size of iris data and to prevent the visibility of iris images, we introduce the idea of 2D Fourier Phase Code (FPC) for representing iris information. The 2D FPC is particularly useful for implementing compact iris recognition devices using state-of-the-art Digital Signal Processing (DSP) technology.

Index Terms—Phase-based image matching, phase-only correlation, phase-only matched filtering, biometrics, iris recognition.

1 Introduction

Biometric authentication has been receiving extensive attention over the last decade, with increasing demands in automated personal identification. The aim of biometrics is to identify individuals using physiological or behavioral characteristics such as fingerprints, face, iris, retina, and palmprints. Among many biometric techniques, iris recognition is one of the most promising approaches due to its high reliability for personal identification [1], [2], [3], [4], [5], [6], [7], [8], [9].

The human iris, which is the annular part between the pupil and the white sclera, has a complex pattern determined by the chaotic morphogenetic processes during embryonic development. The iris pattern is unique to each person and to each eye and is essentially stable over a lifetime. Furthermore, an iris image is typically captured using a noncontact imaging device, which is of great importance in practical applications.

A major approach for iris recognition today is to generate feature vectors corresponding to individual iris images and to perform iris matching based on some distance metrics [3], [4], [5], [6]. Most of the commercial iris recognition systems implement a famous algorithm using *iriscode*, which was proposed by Daugman [3]. In this algorithm, 2D Gabor filters are used to extract a feature vector corresponding to a given iris image. Then, the filter outputs are quantized to generate a 2 Kbit iriscode. The dissimilarity between a pair of iriscodes is measured by their Hamming distance based on an exclusive-OR operation. The iriscode is very compact and can be accommodated, even on the magnetic stripe implemented on the back of typical credit cards. In addition, exclusive-OR comparison allows us to perform extremely rapid recognition. On the other hand, one of the difficult problems in feature-based iris recognition is that the matching performance is significantly influenced by many parameters in the feature extraction process (for example, spatial position, orientation, center frequencies, and size parameters for 2D Gabor filter kernels), which may vary, depending on the environmental factors of iris image acquisition. Given a set of test iris images, extensive parameter optimization is required to achieve a higher recognition rate.

Addressing the above problem, this paper proposes an efficient iris recognition algorithm using phase-based image matching, that is, an image matching technique using only the phase components in 2D Discrete Fourier Transforms (DFTs) of given images. The technique of phase-based image matching has so far been successfully applied to high-accuracy image registration tasks for computer vision applications [10], [11], [12], where the estimation of subpixel image translation is a major concern. In our previous work [13], [14], [15], [16], on the other hand, we proposed an efficient fingerprint recognition algorithm using phase-based image matching and we have developed commercial fingerprint verification units for access-control applications [17]. The original contribution of this paper is to show that the same matching technique is also highly effective for iris recognition (see our conference papers [18], [19] for earlier discussions of the proposed idea). Experimental evaluation using the CASIA iris image databases (versions 1.0 and 2.0) [20] and Iris Challenge Evaluation (ICE) 2005 database [21] clearly demonstrates that the use of the Fourier phase spectra of iris images makes it possible to achieve highly accurate iris recognition with a simple matching algorithm.

- *K. Miyazawa, K. Ito, and T. Aoki are with the Graduate School of Information Sciences, Tohoku University, Aoba 6-6-05, Aramaki, Aoba-ku, Sendai 980-8579, Japan.*
  E-mail: {miyazawa, ito}@aoki.ecei.tohoku.ac.jp, aoki@ecei.tohoku.ac.jp.
- *K. Kobayashi and H. Nakajima are with Yamatake Corporation, Kawana 1-12-2, Fujisawa 251-8522, Japan.*
  E-mail: {kobayashi-koji, nakajima-hiroshi-1}@jp.yamatake.com.

Manuscript received 7 Feb. 2006; revised 25 Oct. 2006; accepted 1 Nov. 2007; published online 29 Nov. 2007.
Recommended for acceptance by P.J. Phillips.
For information on obtaining reprints of this article, please send e-mail to: tpami@computer.org, and reference IEEECS Log Number TPAMI-0136-0206.
Digital Object Identifier no. 10.1109/TPAMI.2007.70833.

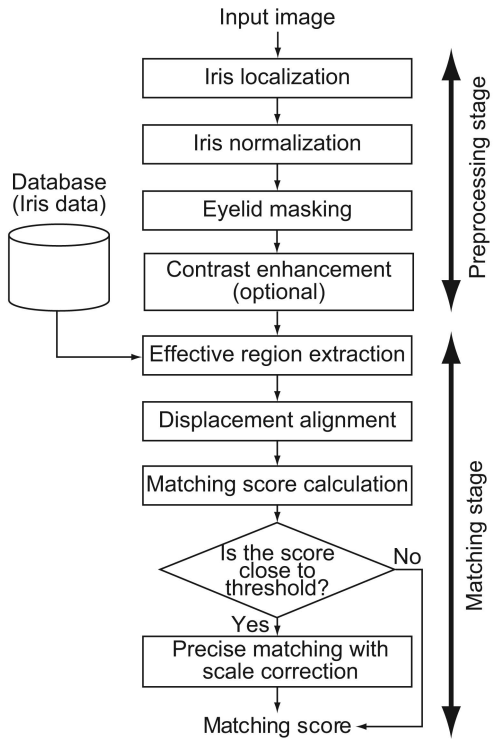

Fig. 1. Flow diagram of the proposed algorithm.

This paper also discusses the major implementation issues of our algorithm. The proposed matching algorithm assumes the use of iris images registered in the system to achieve high performance. In order to reduce the size of iris data and to prevent the visibility of individual iris images, we introduce the idea of 2D Fourier Phase Code (FPC) for representing iris information. The 2D FPC is particularly useful for implementing compact iris recognition devices using the state-of-the-art Digital Signal Processing (DSP) technology. By changing the degree of phase quantization, we can optimize the trade-off between iris data size and recognition performance flexibly while avoiding the visibility of individual iris images.

2 Preprocessing

Fig. 1 shows the overview of the proposed algorithm. The algorithm consists of two stages: 1) the preprocessing stage and 2) the matching stage. The purpose of preprocessing is to localize the iris region in the captured image and to produce a normalized iris texture image with a fixed size (256×128 pixels in our algorithm). A typical eye image contains some irrelevant parts (for example, the eyelid, sclera, and pupil), which cause significant degradation of the matching performance. The preprocessing step is designed to remove these irrelevant parts correctly from the given image and to extract only the iris region. In addition, the size of the extracted iris varies, depending on the camera-to-eye distance and light brightness level, as schematically illustrated in Fig. 2. Therefore, the size should be normalized before the matching operation.

2.1 Iris Localization

This step detects the inner boundary (the boundary between the iris and the pupil) and the outer boundary (the boundary between the iris and the sclera) in the

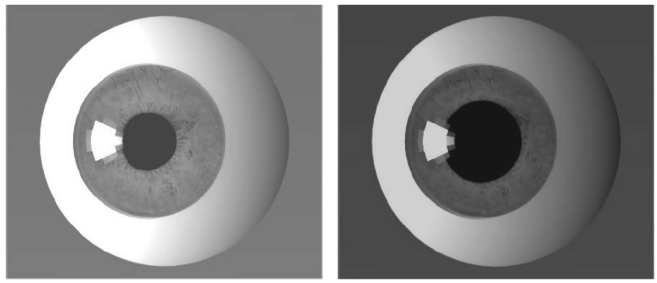

(a) (b)

Fig. 2. Iris size change, depending on the brightness level: (a) bright and (b) dark.

original gray-scale image $f_{org}(m_1, m_2)$ shown in Fig. 3a. Fig. 4 shows the deformable iris model with 10 parameters used in our system, where the inner boundary and the outer boundary of an iris are represented by a pair of independent ellipses. Through a set of experiments, we found that the accuracy of the iris localization step has significant impact on the overall system performance. Hence, the highly flexible iris model with 10 parameters is employed in our system.

Listed as follows are the detailed steps of the inner boundary detection:

1. The first step is to detect the pupil center (c_1, c_2) in the original image $f_{org}(m_1, m_2)$. To do this, we first transform the given gray-scale image $f_{org}(m_1, m_2)$ into a binary (negative) image $f_{bin}(m_1, m_2)$, where the pixel value 1 corresponds to the dark pixel and the value 0 corresponds to the bright pixel. Then, the pupil center (c_1, c_2) is estimated as the center of gravity of the binary image $f_{bin}(m_1, m_2)$ defined as follows:

$$c_1 = \frac{\sum_{(m_1,m_2)\in W} m_1 f_{bin}(m_1, m_2)}{\sum_{(m_1,m_2)\in W} f_{bin}(m_1, m_2)}, \quad (1)$$

$$c_2 = \frac{\sum_{(m_1,m_2)\in W} m_2 f_{bin}(m_1, m_2)}{\sum_{(m_1,m_2)\in W} f_{bin}(m_1, m_2)}. \quad (2)$$

The coordinates (c_1, c_2) are updated repeatedly by reducing the size of the search area W until they converge to a certain point. For every iteration, the search area W is shifted to the updated pupil center (c_1, c_2). In addition, the size of W is reduced until it covers the whole pupil region with a moderate margin. The obtained coordinates (c_1, c_2) for the pupil center are used as the initial values for the optimization in Step 2.

The accuracy of pupil center detection depends on the threshold value used for image binarization. That is, if many nonpupil regions (for example, the eyelashes) have pixel value 1 (that is, a dark pixel) in the binary image $f_{bin}(m_1, m_2)$, (1) and (2) may choose a pixel (c_1, c_2) that is in the nonpupil region, resulting in false detection of the inner boundary in Step 2. Thus, it is important to determine the appropriate threshold value for binarization. For

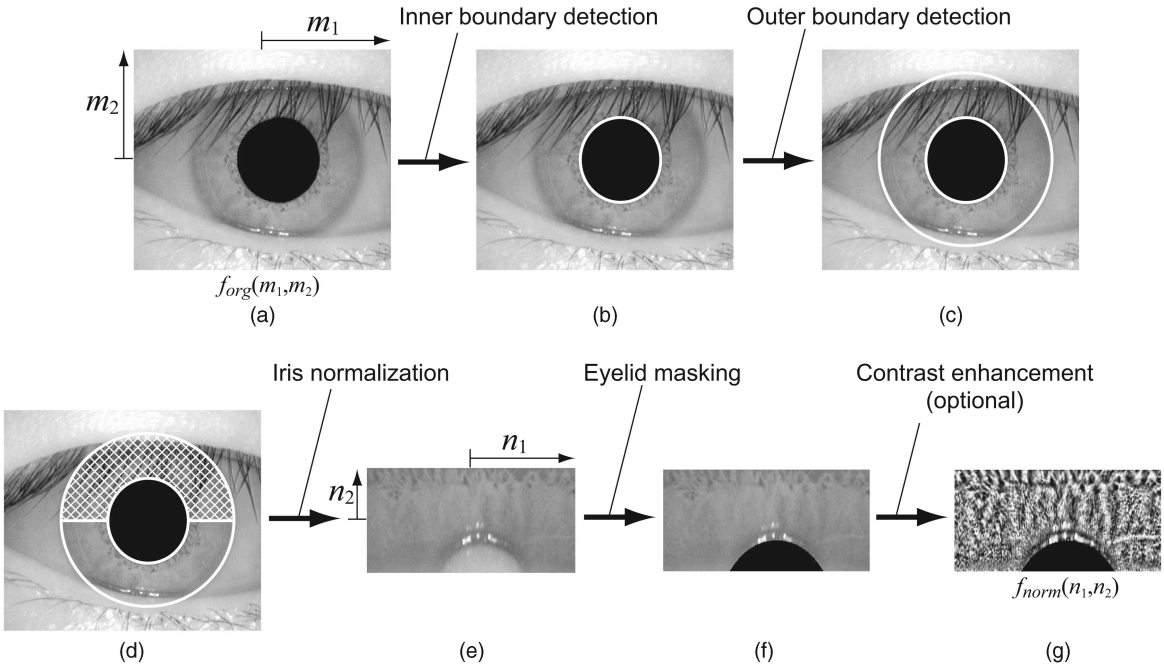

Fig. 3. Iris image preprocessing. (a) Original image $f_{org}(m_1, m_2)$. (b) Detected inner boundary. (c) Detected outer boundary. (d) Lower half of the iris region for matching. (e) Normalized image. (f) Normalized image with eyelid masking. (g) Enhanced image $f_{norm}(n_1, n_2)$.

example, in our experiments with the CASIA version 1.0 database, we determine the threshold value from the intensity histogram of the original image since the pupil regions in the iris images of this database have constant intensity values which can be easily identified in the histograms. For the CASIA version 2.0 and ICE 2005 databases, on the other hand, we first detect the corneal reflection in the iris image and then we determine the binarization threshold from pixel values around the detected corneal area. As a result, we can estimate the pupil region without significant error.

2. The next step is to find the optimal estimate $(l_1, l_2, c_1, c_2, \theta_1)$ for the inner boundary (Fig. 4) by maximizing the following absolute difference:

$$|S(l_1 + \Delta l_1, l_2 + \Delta l_2, c_1, c_2, \theta_1) - S(l_1, l_2, c_1, c_2, \theta_1)|. \quad (3)$$

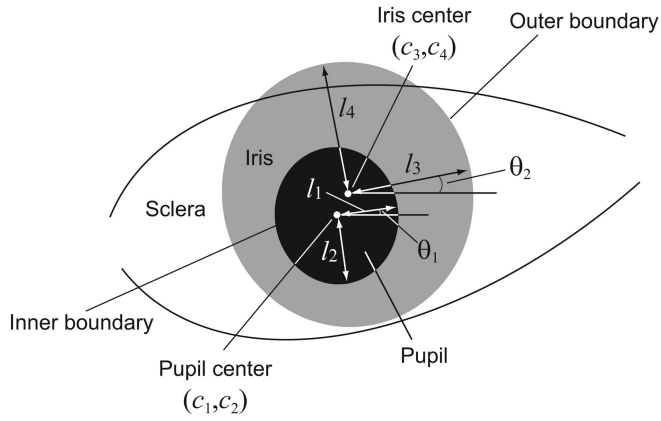

Fig. 4. Deformable iris model with 10 parameters.

Here, Δl_1 and Δl_2 are small constant, and S denotes the N-point contour summation of pixel values along the ellipse and is defined as

$$S(l_1, l_2, c_1, c_2, \theta_1) = \sum_{n=0}^{N-1} f_{org}(p_1(n), p_2(n)), \quad (4)$$

where $p_1(n) = l_1 \cos\theta_1 \cdot \cos(\frac{2\pi}{N} n) - l_2 \sin\theta_1 \cdot \sin(\frac{2\pi}{N} n) + c_1$ and $p_2(n) = l_1 \sin\theta_1 \cdot \cos(\frac{2\pi}{N} n) + l_2 \cos\theta_1 \cdot \sin(\frac{2\pi}{N} n) + c_2$. Thus, we will detect the inner boundary as the ellipse on the image for which there will be a sudden change in luminance summed around its perimeter. Fig. 3b shows an example of inner boundary detection. In order to reduce the computation time, the parameter set $(l_1, l_2, c_1, c_2, \theta_1)$ can be simplified, depending on iris images. For example, in our experiments using the CASIA iris image databases (versions 1.0 and 2.0) and ICE 2005 database, assuming $\theta_1 = 0$ causes no degradation in its performance.

The optimal estimate $(l_3, l_4, c_3, c_4, \theta_2)$ for the outer boundary (Fig. 4), on the other hand, can be found in the same manner, with the path of contour summation simplified from an ellipse to a circle (that is, $l_3 = l_4$). Fig. 3c shows an example of outer boundary detection. This iris localization algorithm could be applied to many difficult eye images and some examples are shown in Fig. 5.

2.2 Iris Normalization

The next step is to normalize the extracted iris region and to compensate for the elastic deformations in iris texture. We unwrap the iris region to a normalized rectangular block with a fixed size (256 × 128 pixels in our experiments). To avoid having the iris region be occluded by the upper eyelid and eyelashes, we use only the lower half of the iris region, as shown in Fig. 3d. This iris

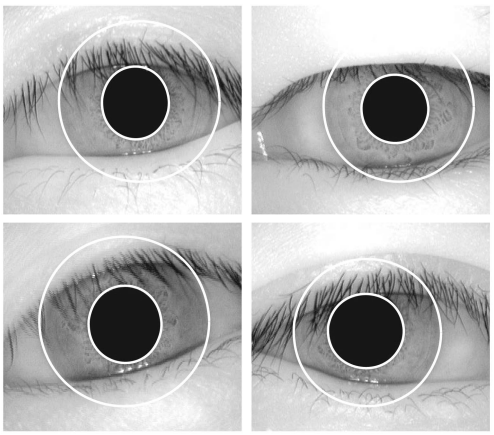

Fig. 5. Examples of iris localization.

region is transformed into the normalized image by the parameters $(l_1, l_2, l_3, l_4, c_1, c_2, c_3, c_4, \theta_1, \theta_2)$, as shown in Fig. 3e, where the n_1 axis corresponds to the angle of the polar coordinate system and the n_2 axis corresponds to the radius.

2.3 Eyelid Masking

This process masks the irrelevant eyelid region in the normalized iris image. In general, the iris/eyelid boundary can be modeled as an ellipse contour in the normalized image. Hence, the same method for detecting the inner boundary can be applied to iris/eyelid boundary detection. The detected eyelid region is masked as shown in Fig. 3f.

2.4 Contrast Enhancement

In some situations, the normalized iris image has low contrast. Typical examples of low-contrast iris images are found in the CASIA version 2.0 and ICE 2005 databases. In such a case, we improve the contrast by using the local histogram equalization technique [22]. Histogram equalization transforms the pixel value so that the resulting image has an approximately flat histogram. To do this, we use a cumulative histogram of the image as the pixel value mapping function. Let $H(u)$ be the cumulative histogram of the image, where u denotes the pixel value ($\in [0, 255]$). We convert the pixel value u in the iris image to the pixel value $255H(u)/N_{total}$ to have a contrast-enhanced iris image, where N_{total} denotes the total counts of pixels. In our algorithm, we transform the pixel value by using the local cumulative histogram evaluated within a small image block (of size 15×15 pixels) centered at the pixel to be converted. Fig. 3g shows an enhanced image, where the iris texture becomes much clearer than in Fig. 3f.

3 Fundamentals of Phase-Based Image Matching

The key idea in this paper is to use phase-based image matching for the matching stage shown in Fig. 1. Before discussing the details of the matching algorithm (in Section 4), this section introduces the principle of phase-based image matching using the Phase-Only Correlation (POC) function [11], [12], [13], [14], [15], [16].

Consider two $N_1 \times N_2$ images $f(n_1, n_2)$ and $g(n_1, n_2)$, where we assume that the index ranges are $n_1 = -M_1, \cdots, M_1$ $(M_1 > 0)$ and $n_2 = -M_2, \cdots, M_2$ $(M_2 > 0)$ for mathematical simplicity[1] and, hence, $N_1 = 2M_1 + 1$ and $N_2 = 2M_2 + 1$. Let $F(k_1, k_2)$ and $G(k_1, k_2)$ denote the 2D DFTs of the two images. $F(k_1, k_2)$ and $G(k_1, k_2)$ are given by

$$\begin{aligned} F(k_1, k_2) &= \sum_{n_1=-M_1}^{M_1} \sum_{n_2=-M_2}^{M_2} f(n_1, n_2) W_{N_1}^{k_1 n_1} W_{N_2}^{k_2 n_2} \\ &= A_F(k_1, k_2) e^{j\theta_F(k_1, k_2)}, \end{aligned} \tag{5}$$

$$\begin{aligned} G(k_1, k_2) &= \sum_{n_1=-M_1}^{M_1} \sum_{n_2=-M_2}^{M_2} g(n_1, n_2) W_{N_1}^{k_1 n_1} W_{N_2}^{k_2 n_2} \\ &= A_G(k_1, k_2) e^{j\theta_G(k_1, k_2)}, \end{aligned} \tag{6}$$

where $k_1 = -M_1, \cdots, M_1$, $k_2 = -M_2, \cdots, M_2$, $W_{N_1} = e^{-j\frac{2\pi}{N_1}}$, and $W_{N_2} = e^{-j\frac{2\pi}{N_2}}$. $A_F(k_1, k_2)$ and $A_G(k_1, k_2)$ are amplitude components and $\theta_F(k_1, k_2)$ and $\theta_G(k_1, k_2)$ are phase components. The cross-phase spectrum $R_{FG}(k_1, k_2)$ between $F(k_1, k_2)$ and $G(k_1, k_2)$ is given by

$$\begin{aligned} R_{FG}(k_1, k_2) &= \frac{F(k_1, k_2)\overline{G(k_1, k_2)}}{|F(k_1, k_2)\overline{G(k_1, k_2)}|} \\ &= e^{j\{\theta_F(k_1, k_2) - \theta_G(k_1, k_2)\}}, \end{aligned} \tag{7}$$

where $\overline{G(k_1, k_2)}$ denotes the complex conjugate of $G(k_1, k_2)$. The POC function $r_{fg}(n_1, n_2)$ is the 2D Inverse DFT (IDFT) of $R_{FG}(k_1, k_2)$ and is given by

$$\begin{aligned} r_{fg}(n_1, n_2) = \frac{1}{N_1 N_2} \sum_{k_1=-M_1}^{M_1} \sum_{k_2=-M_2}^{M_2} R_{FG}(k_1, k_2) \\ \times W_{N_1}^{-k_1 n_1} W_{N_2}^{-k_2 n_2}. \end{aligned} \tag{8}$$

When two images are similar, their POC function gives a distinct sharp peak. When $f(n_1, n_2) = g(n_1, n_2)$, the POC function $r_{fg}(n_1, n_2)$ becomes the Kronecker delta function $\delta(n_1, n_2)$. If two images are not similar, the peak value drops significantly. The height of the peak can be used as a good similarity measure for image matching and the location of the peak shows the translational displacement between the two images.

In our previous work on fingerprint recognition [13], [14], [15], we proposed the idea of the Band-Limited POC (BLPOC) function for an efficient matching of fingerprints, considering the inherent frequency components of fingerprint images. Through a set of experiments, we have found that the same idea is also very effective for iris recognition. Our observation shows that the 2D DFT of a normalized iris image sometimes includes meaningless phase components in high-frequency domains and that the effective frequency band of the normalized iris image is wider in the k_1 direction than in the k_2 direction, as illustrated in Fig. 6. The original POC function $r_{fg}(n_1, n_2)$ emphasizes the high-frequency components, which may have less reliability. This reduces the height of the correlation peak significantly, even if the given two iris images are captured from the same eye. On the other hand, the BLPOC function

1. Note that the discussion could be easily generalized to nonnegative index ranges with power-of-two image sizes.

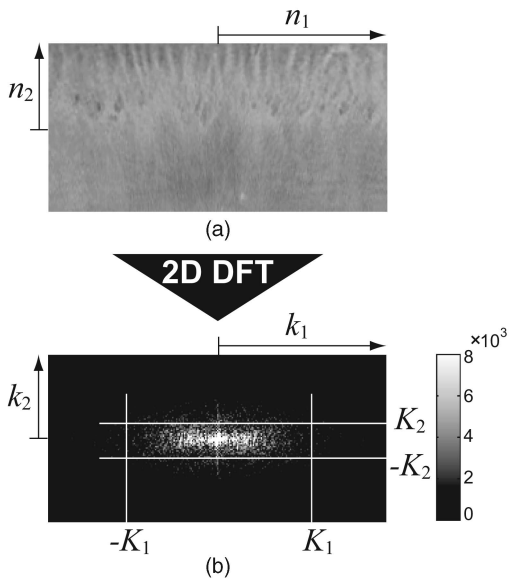

Fig. 6. Normalized iris image in (a) the spatial domain and (b) the frequency domain (amplitude spectrum).

allows us to evaluate the similarity by using the inherent frequency band of the iris texture.

Assume that the ranges of the inherent frequency band of iris texture are given by $k_1 = -K_1, \cdots, K_1$ and $k_2 = -K_2, \cdots, K_2$, where $0 \leq K_1 \leq M_1$, and $0 \leq K_2 \leq M_2$. Thus, the effective size of frequency spectrum is given by $L_1 = 2K_1 + 1$ and $L_2 = 2K_2 + 1$. The BLPOC function is defined as

$$r_{fg}^{K_1K_2}(n_1, n_2) = \frac{1}{L_1 L_2} \sum_{k_1=-K_1}^{K_1} \sum_{k_2=-K_2}^{K_2} R_{FG}(k_1, k_2) \times W_{L_1}^{-k_1 n_1} W_{L_2}^{-k_2 n_2}, \quad (9)$$

where $n_1 = -K_1, \cdots, K_1$, and $n_2 = -K_2, \cdots, K_2$. When two images are similar, their BLPOC function gives a distinct sharp peak. When $f(n_1, n_2) = g(n_1, n_2)$, we have $r_{fg}^{K_1K_2}(n_1, n_2) = \delta(n_1, n_2)$. Note that the maximum value of the correlation peak of the BLPOC function is always normalized to 1 and does not depend on L_1 and L_2. In addition, the translational displacement between the two images can be estimated by the correlation peak position.

In our matching algorithm, K_1/M_1 and K_2/M_2 are the major control parameters since these parameters reflect the quality of iris images. In other words, we need to select adequate values of these parameters, depending on the iris database to be used. In our experiments, we use the parameter set $(K_1/M_1, K_2/M_2) = (0.6, 0.2)$ for the CASIA version 1.0 database, $(K_1/M_1, K_2/M_2) = (0.55, 0.2)$ for the CASIA version 2.0 database, and $(K_1/M_1, K_2/M_2) = (0.4, 0.2)$ for the ICE 2005 database.

Figs. 7 and 8 show examples of genuine and impostor matching, respectively, in the CASIA iris image version 1.0 database, where each figure compares the original POC function $r_{fg}(n_1, n_2)$ and the BLPOC function $r_{fg}^{K_1K_2}(n_1, n_2)$. In the case of genuine matching, the BLPOC function exhibits a higher correlation peak than that of the original POC function, while, with impostor matching, neither function shows significant correlation. Thus, the BLPOC function provides a much higher discrimination capability than the original POC function.

In practical iris recognition tasks, we need to determine an appropriate threshold for the peak value of the BLPOC function in order to distinguish authorized from unauthorized people. Given a set of test iris images, we can determine the optimal value of threshold from Receiver Operating Characteristic (ROC) curves. Section 5 discusses the detailed performance assessment of our algorithms based on the ROC curves. Typical threshold values at the Equal Error Rate (EER) condition are given by 0.15 for the CASIA version 1.0 database, 0.095 for the CASIA version 2.0 database, and 0.079[2] for the ICE 2005 database.

4 Matching Algorithms

In this section, we describe the detailed process of the matching stage in Fig. 1, which consists of effective region extraction (to be explained in Section 4.1.1), image alignment (to be explained in Section 4.1.2), and matching score calculation (to be explained in Sections 4.1.3 and 4.1.4). Sections 4.1.1-4.1.4 form a baseline matching algorithm. The BLPOC function described in Section 3 is used in image alignment and matching score calculation. In Section 4.2, on the other hand, we modify the baseline matching algorithm so as to deal with significantly degraded iris images.

4.1 Baseline Algorithm

4.1.1 Effective Region Extraction

Given a pair of normalized iris images $f_{norm}(n_1, n_2)$ and $g_{norm}(n_1, n_2)$ to be compared, the purpose of this process is to extract effective regions of the same size from the two images, as illustrated in Fig. 9a. Let the size of two images $f_{norm}(n_1, n_2)$ and $g_{norm}(n_1, n_2)$ be $N_1 \times N_2$ and let the heights of irrelevant regions in $f_{norm}(n_1, n_2)$ and $g_{norm}(n_1, n_2)$ be h_f and h_g, respectively. We obtain effective images $f_{eff}(n_1, n_2)$ and $g_{eff}(n_1, n_2)$ by extracting effective regions of size $N_1 \times \{N_2 - \max(h_f, h_g)\}$. We eliminate irrelevant regions such as a masked eyelid and specular reflections.

On the other hand, a problem may occur when most of the normalized iris image is covered by the eyelid (that is, when $\max(h_f, h_g) \simeq N_2$). In such a case, the extracted region becomes too small to perform image matching. To solve this problem, we extract multiple effective subregions from each iris image by changing the height parameter h, as illustrated in Fig. 9b. In our experiments, we extract six subregions from a single iris image by changing the parameter h as 55, 75, and 95 pixels. Our experimental observation shows that the recognition performance of the proposed algorithm is not sensitive to these values. Thus, we do not perform optimization for the parameter h.

4.1.2 Displacement Alignment

This step aligns the translational displacement (τ_1, τ_2) between the extracted images $f_{eff}(n_1, n_2)$ and $g_{eff}(n_1, n_2)$. The rotation of the camera, head tilt, and rotation of the eye within the eye socket may cause displacements in normalized

2. The typical threshold value for the ICE 2005 database is derived from the result of Experiment 1 (see Section 5 for our experimental condition).

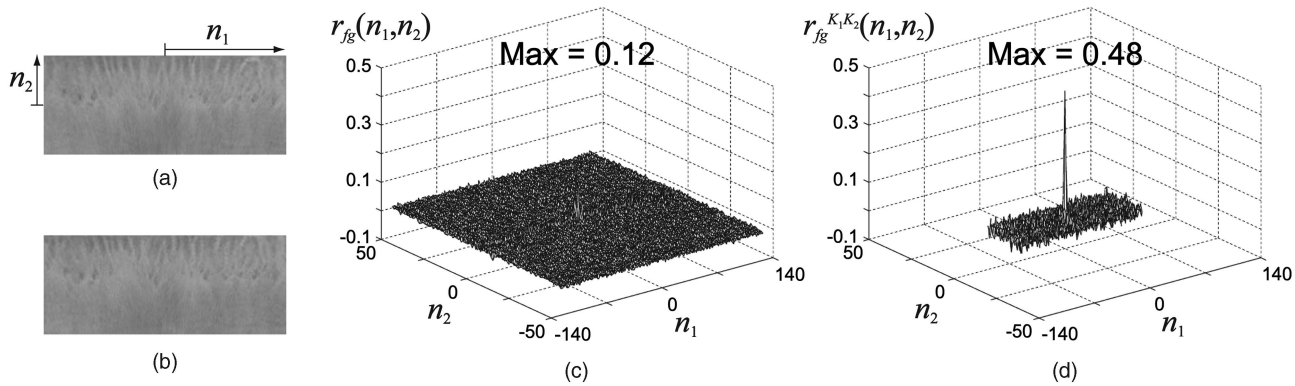

Fig. 7. Example of genuine matching using the original POC function and the BLPOC function. (a) Iris image $f(n_1, n_2)$. (b) Iris image $g(n_1, n_2)$. (c) Original POC function $r_{fg}(n_1, n_2)$. (d) BLPOC function $r_{fg}^{K_1K_2}(n_1, n_2)$ $(K_1/M_1 = 0.6, K_2/M_2 = 0.2)$.

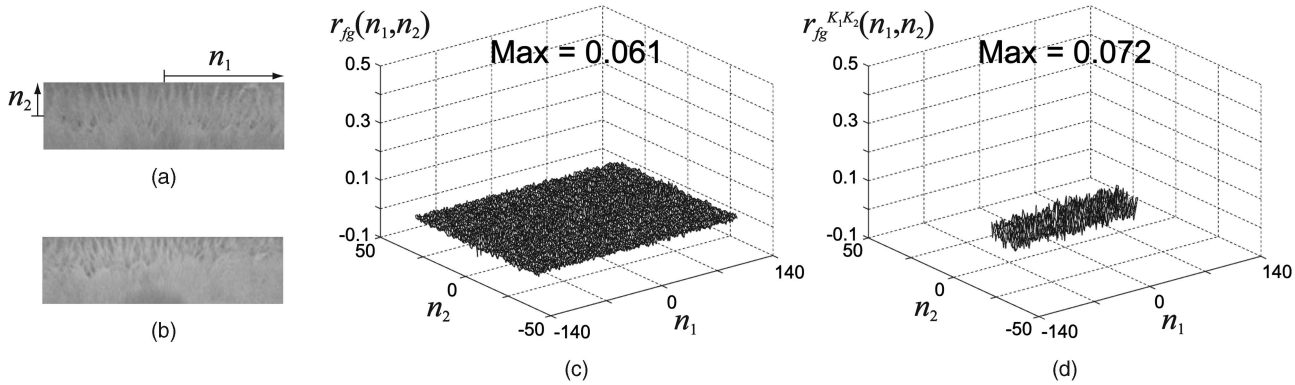

Fig. 8. Example of impostor matching using the original POC function and the BLPOC function. (a) Iris image $f(n_1, n_2)$. (b) Iris image $g(n_1, n_2)$. (c) Original POC function $r_{fg}(n_1, n_2)$. (d) BLPOC function $r_{fg}^{K_1K_2}(n_1, n_2)$ $(K_1/M_1 = 0.6, K_2/M_2 = 0.2)$.

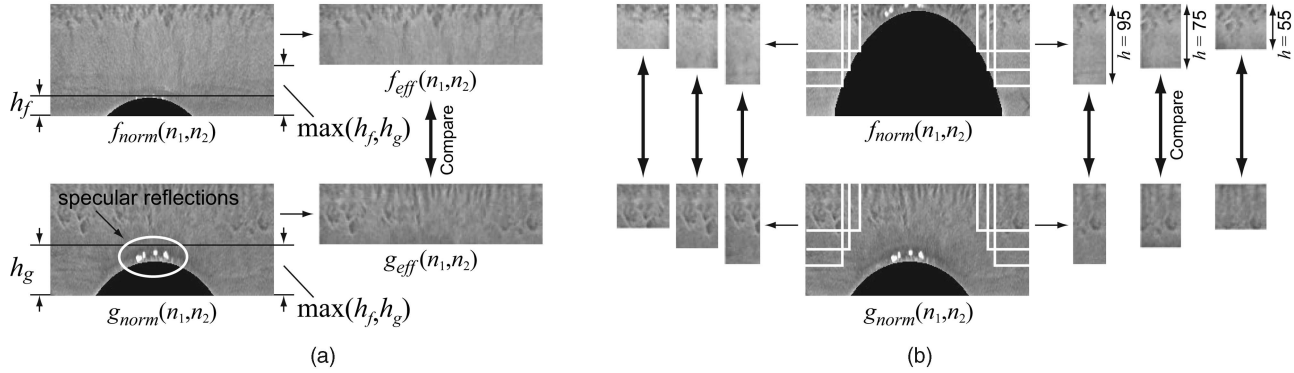

Fig. 9. Effective region extraction. (a) Normal case. (b) The case when multiple subregions should be extracted.

images (due to the polar coordinate transformation). The displacement (τ_1, τ_2) can be estimated from the peak location of the BLPOC function $r_{f_{eff}g_{eff}}^{K_1K_2}(n_1, n_2)$. We align the two images based on the parameter set (τ_1, τ_2) and extract common-region images $f(n_1, n_2)$ and $g(n_1, n_2)$.

4.1.3 Matching Score Calculation

In this step, we calculate the BLPOC function $r_{fg}^{K_1K_2}(n_1, n_2)$ between the aligned images $f(n_1, n_2)$ and $g(n_1, n_2)$ and we evaluate the matching score. In the case of genuine matching, if the displacement between the two images is aligned, the correlation peak of the BLPOC function should appear at the origin $(n_1, n_2) = (0, 0)$. Thus, we calculate the matching score between the two images as the maximum peak value of the BLPOC function within the small window O centered at the origin. The matching score is given by

$$\text{Matching score} = \max_{(n_1,n_2)\in O}\left\{r_{fg}^{K_1K_2}(n_1, n_2)\right\}. \tag{10}$$

In our experiments, the size of the window O is 11×11 pixels. When multiple subregions are extracted at the "*Effective region extraction*" process, as shown in Fig. 9b, the matching score is calculated by taking an average of matching scores for six subregions.

4.1.4 Precise Matching with Scale Correction

For some iris images, errors take place in the iris localization process. This error causes slight scaling in the horizontal direction (that is, the n_1 direction) of the

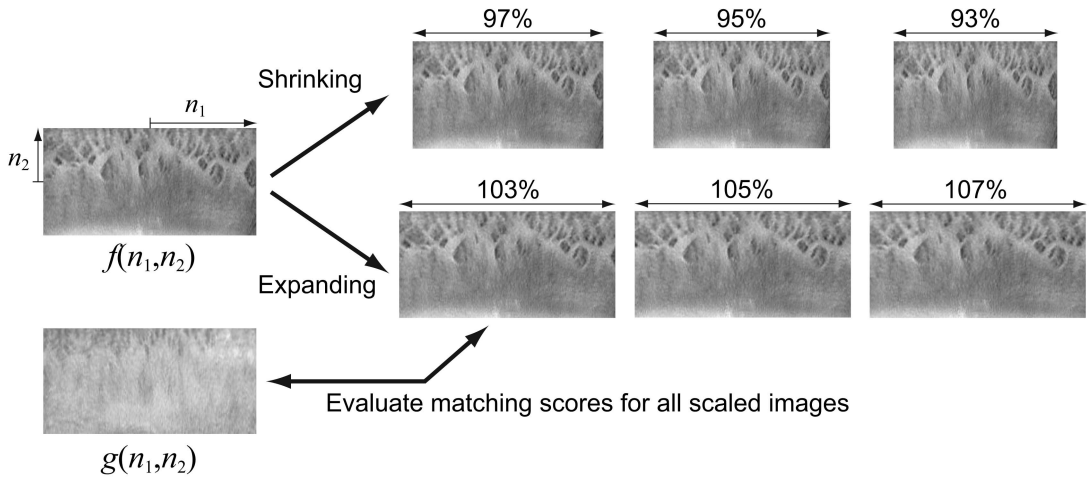

Fig. 10. Precise matching with scale correction.

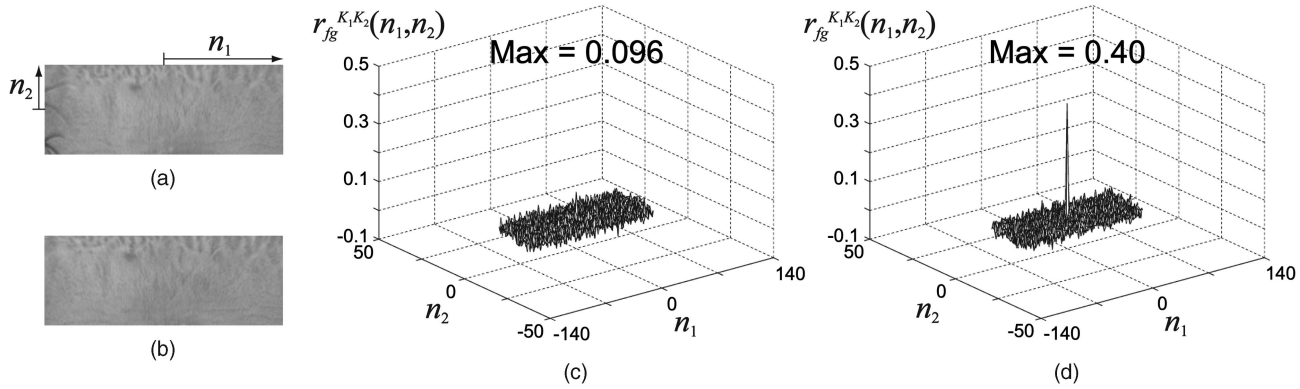

Fig. 11. Effect of scale correction in genuine matching. (a) Iris image $f(n_1, n_2)$. (b) Iris image $g(n_1, n_2)$. (c) BLPOC function without scale correction. (d) BLPOC function with scale correction.

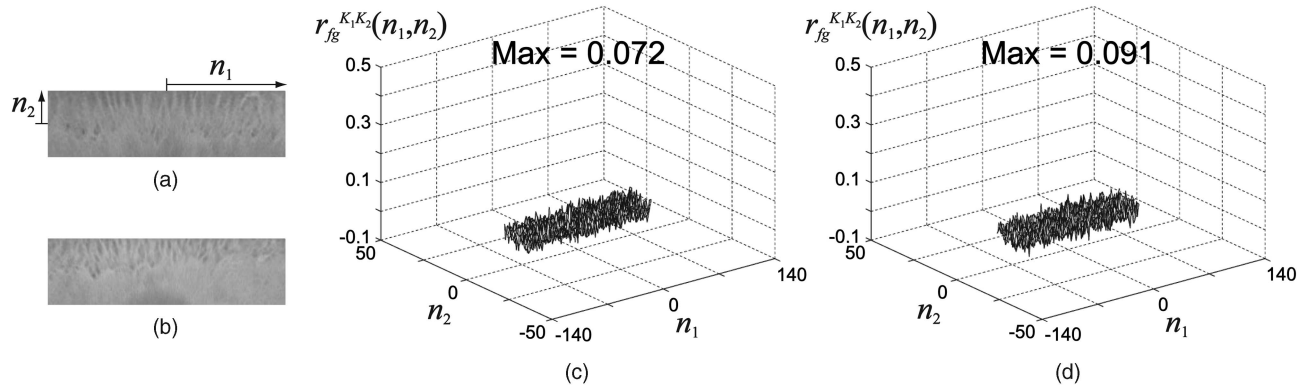

Fig. 12. Effect of scale correction in impostor matching. (a) Iris image $f(n_1, n_2)$. (b) Iris image $g(n_1, n_2)$. (c) BLPOC function without scale correction. (d) BLPOC function with scale correction.

normalized iris image. In the case of the genuine matching, this reduces the height of the correlation peak. Thus, if the matching score is close to the threshold value to separate genuine scores and impostor scores, we generate a set of slightly scaled images, calculate the matching scores for the generated images, and select their maximum value as the final matching score. In our experiments, we scale the normalized images in the n_1 direction by ± 3 percent, ± 5 percent, and ± 7 percent, as illustrated in Fig. 10. The effects of scale correction in genuine matching and in impostor matching are shown in Figs. 11 and 12, respectively. In the case of genuine matching, the correlation peak value of the BLPOC function is enhanced. On the other hand, with impostor matching, there is no significant change in the peak value.

4.2 Modified Algorithm for Degraded Iris Images

This section presents some modifications of the baseline matching algorithm which are especially suitable for degraded iris images. The baseline algorithm described in the previous section performs image matching only once by using the whole iris image, as shown in Figs. 7 and 8 (except for the case in Fig. 9b). If the quality of iris images is sufficient, a single matching is enough to achieve a highly

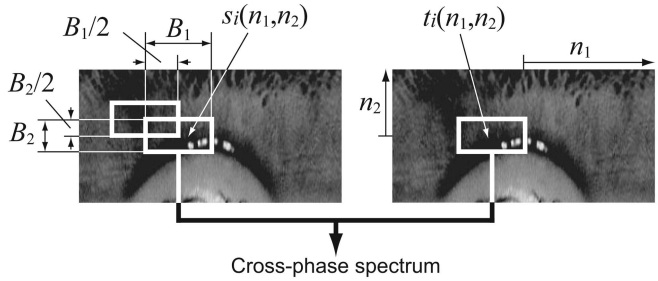

Fig. 13. Block partitioning and cross-phase spectrum calculation.

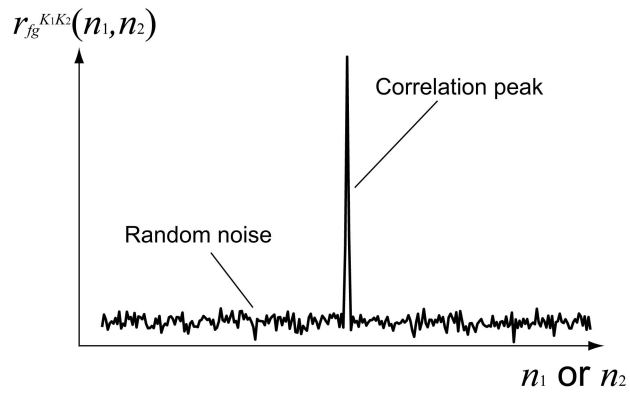

Fig. 14. Schematic illustration of the BLPOC function.

accurate iris recognition. When the quality of iris images is significantly degraded due to, for example, defocusing and blurring, it is difficult to achieve high performance by the baseline algorithm. Addressing this problem, we modify the matching algorithm by introducing a spatial ensemble averaging of the BLPOC function. Given a pair of iris images, we first divide each iris image into multiple small blocks (that is, subregions) and compute the BLPOC function for every block pair. Then, we take an average of the computed BLPOC functions across the whole image plane to improve the peak-to-noise ratio of the correlation surface. This technique leads to better discrimination capability, even for highly degraded iris images.

In Sections 4.2.1-4.2.3, we explain the detailed process of the modified algorithm. The algorithm starts with the two normalized iris images $f_{norm}(n_1, n_2)$ and $g_{norm}(n_1, n_2)$. Unlike the baseline algorithm, the modified algorithm does not perform eyelid masking and effective region extraction and is given as follows:

4.2.1 Displacement Alignment

This process aligns the translational displacement (τ_1, τ_2) between $f_{norm}(n_1, n_2)$ and $g_{norm}(n_1, n_2)$. We obtain the aligned images $f(n_1, n_2)$ and $g(n_1, n_2)$ by using the same idea described in Section 4.1.2.

4.2.2 Block Partitioning and Cross-Phase Spectrum Calculation

We first partition the aligned iris images $f(n_1, n_2)$ and $g(n_1, n_2)$ into multiple blocks. Assume that the size of a block is $B_1 \times B_2$ pixels (64 × 32 pixels in our experiments) and that each block overlaps with the adjacent blocks by $B_1/2$ pixels in the n_1 direction and by $B_2/2$ pixels in the n_2 direction, as illustrated in Fig. 13. Let $s_i(n_1, n_2)$ be the ith block extracted from the image $f(n_1, n_2)$ and $t_i(n_1, n_2)$ be the ith block extracted from the image $g(n_1, n_2)$, where $i = 1, \cdots, N_{block}$. We compute the 2D DFTs of $s_i(n_1, n_2)$ and $t_i(n_1, n_2)$, which are denoted by $S_i(k_1, k_2)$ and $T_i(k_1, k_2)$, respectively. Then, we calculate the cross-phase spectrum $R_{S_iT_i}(k_1, k_2)$ between $S_i(k_1, k_2)$ and $T_i(k_1, k_2)$ according to (7) for every i. The BLPOC function $r_{s_it_i}^{K_1K_2}(n_1, n_2)$ is defined as the 2D IDFT of $R_{S_iT_i}(k_1, k_2)$ (see (9)).

4.2.3 Block-Based Averaging of the Band-Limited Phase-Only Correlation Function and Matching Score Calculation

In this step, we calculate the weighted average of the BLPOC functions $r_{s_it_i}^{K_1K_2}(n_1, n_2)$ $(i = 1, \cdots, N_{block})$ evaluated from all block pairs. The weight w_i associated with the ith BLPOC function $r_{s_it_i}^{K_1K_2}(n_1, n_2)$ is determined depending on the number of irrelevant pixels that belong to the eyelid region in the blocks $s_i(n_1, n_2)$ and $t_i(n_1, n_2)$. Assume that the number of pixels of eyelid regions in $s_i(n_1, n_2)$ is given by E_{s_i} and that, in $t_i(n_1, n_2)$, it is given by E_{t_i}. The weight w_i is defined as

$$w_i = \begin{cases} 1 - \frac{E_i}{B_1 \times B_2} & \text{if } \frac{E_i}{B_1 \times B_2} < 0.5 \\ 0 & \text{otherwise,} \end{cases} \tag{11}$$

where $E_i = \max(E_{s_i}, E_{t_i})$. For computational efficiency, we calculate the weighted average in the frequency domain. The average cross-phase spectrum $R_{ave}(k_1, k_2)$ is given by

$$R_{ave}(k_1, k_2) = \frac{\sum_{i=1}^{N_{block}} w_i R_{S_iT_i}(k_1, k_2)}{\sum_{i=1}^{N_{block}} w_i}. \tag{12}$$

The average BLPOC function $r_{ave}^{K_1K_2}(n_1, n_2)$ is defined as the 2D IDFT of $R_{ave}(k_1, k_2)$ (see (9)). Then, the matching score is calculated by (10), where the size of O is 11 × 7 pixels. As explained in Section 4.1.4, precise matching with scale correction is also performed.

This modification is effective for degraded iris images since the averaging process (12) improves the peak-to-noise ratio of the BLPOC function $r_{ave}^{K_1K_2}(n_1, n_2)$. Fig. 14 illustrates schematically the correlation peak structure of the BLPOC function, where the correlation surface consists of two major components: 1) the *correlation peak* that originated in the correlated image components in iris images and 2) the *random noise* that originated in uncorrelated components. For iris recognition with poor-quality images, reducing the random noise floor is essential since it degrades the impostor rejection rate. The ensemble averaging of correlation surface is highly effective for reducing the noise floor due to uncorrelated components, while it does not affect the correlation peak significantly.

5 Experiments and Discussions

This section describes a set of experiments for evaluating the matching performance of the proposed algorithms, that is, the baseline algorithm described in Section 4.1 and the modified algorithm with averaging described in Section 4.2, using the CASIA iris image databases (versions 1.0 and 2.0) [20] and ICE 2005 database [21]. Note that ICE is the first worldwide iris recognition algorithm competition managed

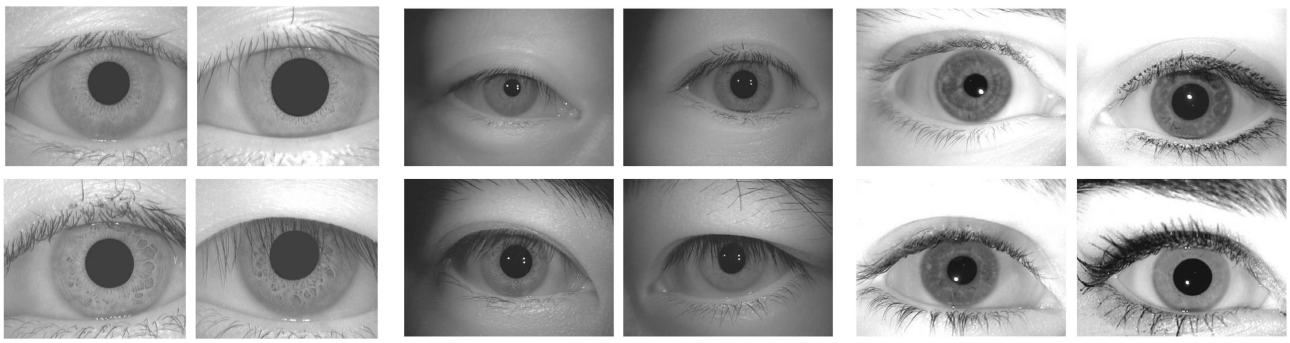

Fig. 15. Examples of iris images in iris image databases. (a) The CASIA iris image version 1.0 database. (b) The CASIA iris image version 2.0 database. (c) The ICE 2005 database.

by the National Institute of Standards and Technology (NIST). Fig. 15 shows some examples of iris images in these databases.

An important advantage of our matching algorithms is that they employ only two main parameters, K_1/M_1 and K_2/M_2, for controlling the iris recognition performance. These parameters may vary depending on the image capture environment and sensors to be used because the parameters reflect the quality of iris images. The parameter K_1/M_1 (or K_2/M_2) corresponds to the effective horizontal (or vertical) bandwidth for iris recognition. That is, for low-quality images without reliable high-frequency components, we should choose small values for K_1/M_1 and K_2/M_2. Thus, there exists a direct relationship between the parameters and the effective frequency spectra of iris images. Due to this simple property, the initial estimate of the optimal parameter set could be easily obtained by examining the amplitude spectra of the given iris images automatically. For the CASIA version 1.0, CASIA version 2.0, and ICE 2005 databases, spectral analysis suggests that the parameters should be around 0.5 for K_1/M_1 and 0.2 for K_2/M_2.

In contrast to the conventional feature-based methods, optimizing these parameters is not a difficult task. Our experimental observation shows that the recognition performance is not so sensitive to K_1/M_1 and K_2/M_2. For example, we employ the parameter sets $(K_1/M_1, K_2/M_2) = (0.6, 0.2)$ for CASIA version 1.0, $(K_1/M_1, K_2/M_2) = (0.55, 0.2)$ for CASIA version 2.0, and $(K_1/M_1, K_2/M_2) = (0.4, 0.2)$ for ICE 2005, even though the image qualities of these databases are significantly different from one another. This invariability of the parameters implies that we do not need to perform extensive parameter optimization, which is usually indispensable in typical feature-based iris recognition algorithms. For each iris image database, we optimize the parameters K_1/M_1 and K_2/M_2 through a set of training trials by changing the parameters as $K_1/M_1 = 0.4, 0.45, 0.5, 0.55, 0.6$ and $K_2/M_2 = 0.2, 0.3$. We select the parameter set achieving the lowest EER. The number of genuine and impostor attempts used in the training process is less than 1 percent of the total number of matching attempts used for performance evaluation. The simplicity of parameter tuning is one of the most important advantages of the proposed iris recognition algorithm.

In the following, we summarize the experimental results of the performance evaluation in the two versions of the CASIA iris image databases and the ICE 2005 database. For each database, we do not specify any training data set for parameter optimization for the above-mentioned reasons. Due to the simplicity of our algorithm, it seems relatively easy for readers to reproduce the experimental results described here in comparison with other typical feature-based approaches:

- CASIA iris image version 1.0 database. This database contains 756 gray-scale eye images (320×280 pixels) with 108 unique eyes and 7 different images of each eye. We first evaluate the genuine (intraclass) matching scores for all the possible combinations of genuine attempts. The number of attempts is ${}_7C_2 \times 108 = 2,268$. Next, we evaluate the impostor (interclass) matching scores for all of the possible combinations of impostor attempts. The number of attempts is ${}_{756}C_2 - 2,268 = 283,122$. Note that the original pupil region of the iris image in this database is edited by CASIA so that the pupil region has a constant "dark" intensity value.[3] This kind of image retouching may have an impact on the accuracy of the performance evaluation. The inner boundary detection described in Section 2.1 becomes easy due to this artificial modification. CASIA version 1.0 is one of the most commonly used iris image databases for evaluation purposes and there are many papers reporting the experimental results on this database. Thus, we use this database in order to compare our experimental results with those reported in other papers.
- CASIA iris image version 2.0 database (device 1). This database contains 1,200 gray-scale eye images (640×480 pixels) with 60 unique eyes and 20 different images of each eye. We first evaluate the genuine (intraclass) matching scores for all of the possible combinations of genuine attempts. The number of attempts is ${}_{20}C_2 \times 60 = 11,400$. Next, we evaluate the impostor (interclass) matching scores for ${}_{60}C_2 \times 4^2 = 28,320$ attempts, where we take four images for each eye and make all of the possible combinations of impostor attempts.

3. During the review process (in August 2006), CASIA released a new database (version 3.0) in which the pupil regions of the iris images are not edited. This database seems to be useful for our future study.

- ICE 2005 database. This database contains 2,953 gray-scale eye images (640×480 pixels) from 124 right eyes and 120 left eyes (1,425 images are from the right eyes and 1,528 images are from the left eyes). In ICE 2005, NIST prepares two different experiments: Experiment 1 (right iris and right iris comparison) and Experiment 2 (left iris and left iris comparison). In these experiments, we should evaluate the genuine and impostor matching scores for all the possible combinations. The number of attempts are given as follows:
  - Experiment 1: 12,214 genuine attempts and 1,002,386 impostor attempts.
  - Experiment 2: 14,653 genuine attempts and 1,151,975 impostor attempts.

  The ICE 2005 database seems to be one of the most challenging iris databases, which includes a variety of iris images with a significant degradation of image quality. The use of the ICE 2005 database is a reasonable approach for evaluating state-of-the-art iris recognition algorithms.

In the experiments using the CASIA version 1.0 database, we compare the performance of the proposed algorithms with those of other approaches published in [4], [9]. In particular, [4] provides a comprehensive survey and systematic performance evaluation of recent iris recognition algorithms and is useful for performance comparison. Both papers are written by Tan et al., who are conducting the CASIA Iris Image Database Project.

For more detailed performance comparison, we use the publicly available Matlab source code of the iris recognition algorithm using 1D log-Gabor filter [23]. This software has been widely used for comparison purposes recently as a Daugman-like algorithm (not exactly Daugman) which produces 1D feature vectors, similar to iriscodes, from individual iris images. In this source code, various parameters have already been optimized for the CASIA iris image version 1.0 database by the author. Thus, we can evaluate the recognition performance directly on CASIA version 1.0. For a fair comparison of iris recognition performance, we utilize the source code in two different ways: 1) The "original test" performs comparison without any modification on the source code and 2) the "modified test" uses the modified source code, in which only the preprocessing stage is modified to our method, while the matching stage remains unchanged. Thus, the modified test allows us to compare only the performance of matching stage.

For the experiments using the ICE 2005 database, we refer to the results of the fully automatic test in ICE 2005 summarized by NIST [24] and compare the performance of our algorithms with those of other state-of-the-art algorithms. In ICE 2005, participants are requested to conduct the experiments by using the ICE 2005 database by themselves and to submit the results to NIST. Then, NIST evaluates the performance of the participants' algorithms based on the submitted results. In our experiments, we follow the instructions of the fully automatic test in ICE 2005 precisely. Note that the main parameters K_1/M_1 and K_2/M_2 are optimized in advance through a set of small training trials using 1,098 genuine attempts and 861 impostor attempts. In our experiments, the ROC curve and EER are used to evaluate the matching performance. The ROC curve illustrates the False Non-Match Rate (FNMR, the probability that an authorized person is falsely rejected) against the False Match Rate (FMR, the probability that a nonauthorized person is falsely accepted as an authorized person) at different thresholds on the matching score. EER indicates the error rate where FNMR and FMR are equal. We evaluate the error rates statistically by using the bootstrap technique [25], which is a nonparametric method to estimate the confidence interval by random data sampling. The bootstrap is only valid if the data is independently and identically distributed. In a biometric recognition system, however, there is statistical dependence among matching scores due to the method of collection of biometric samples. To deal with this kind of dependent data, the modified version of the bootstrap, called "subsets bootstrap," has been proposed [26]. This method groups the set of matching scores by subject or by biometric entity (for example, finger or iris). In our experiments, we use the entity-based subsets bootstrap to calculate the confidence intervals of FNMR and FMR. The procedure for obtaining the confidence interval of FNMR is given as follows:

1. Divide the set of genuine matching scores $\mathbf{X}$ into independent subsets $X_1, \cdots, X_{N_{eye}}$ by eye, where N_{eye} is the number of unique eyes.
2. Generate a bootstrap set $\mathbf{X}^* = \{X_1^*, \cdots, X_{N_{eye}}^*\}$ many times by sampling N_{eye} subsets from $\mathbf{X} = \{X_1, \cdots, X_{N_{eye}}\}$ with replacement, where set $\mathbf{X}^*$ may contain any subset $X_i \ (i = 1, \cdots, N_{eye})$ multiple times or no time. Compute the corresponding bootstrap estimate FNMR^* using the set $\mathbf{X}^*$.

We can calculate the confidence interval of FNMR by using the set of FNMR^*. In our experiments, we repeat Step 2 1,000 times. The confidence interval of FMR is calculated the same way. In the following, the ROC curves are plotted with the 90 percent confidence intervals.

Fig. 16a shows the ROC curves of the proposed algorithms for CASIA version 1.0, where the ROC curves of the 1D log-Gabor-based approaches (the original and modified tests) are also plotted for comparison. As observed in the figure, the proposed algorithms exhibit very low EERs (the baseline is 0.0032 percent, while, with averaging, it is 0.0099 percent) and there is no overlap of confidence intervals between the proposed algorithms and 1D log-Gabor-based approaches. This means that the proposed algorithms achieve significantly higher discrimination capabilities than the 1D log-Gabor methods. The reported values of EER from [4], [9] using the CASIA iris image version 1.0 database are shown in Tables 1 and 2, respectively. It should be noted that the experimental conditions in [4], [9] are not the same as in our case because the complete database is not available at CASIA [20] due to the limitations on usage rights of the iris images. However, the number of iris images accessible from the CASIA Web site [20] (756 iris images) seems large enough for a reasonable performance comparison. (Note that [4] employs 1,237 iris images.) Thus, the proposed algorithms achieve a very low EER compared with other algorithms.

Fig. 16b shows the ROC curves of the proposed algorithms for CASIA version 2.0. Although we cannot find any reliable official report on recognition test for this database, we believe that our result ($\mathrm{EER} = 0.58\%$ for the

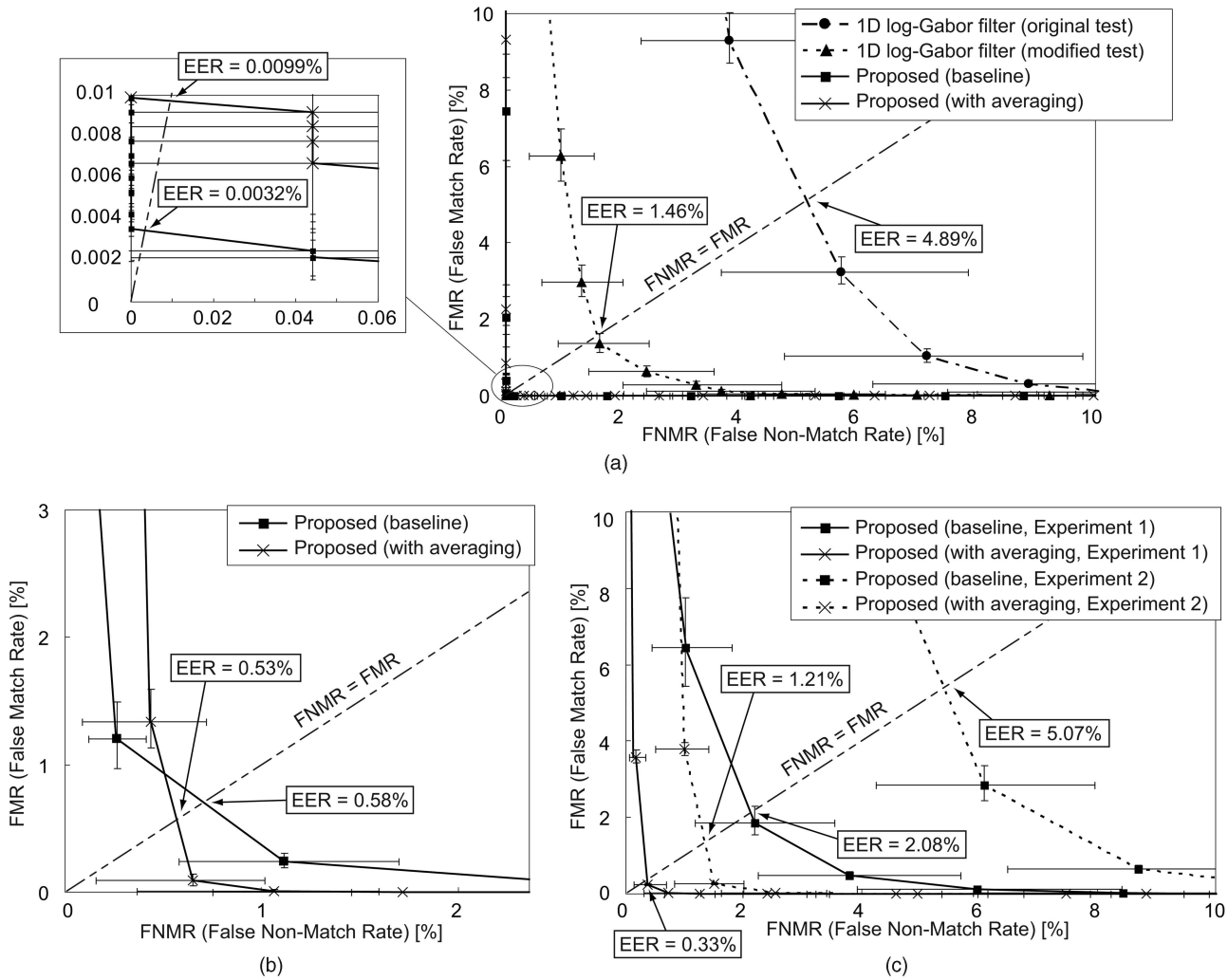

Fig. 16. ROC curves and EERs. (a) The CASIA iris image version 1.0 database. (b) CASIA version 2.0. (c) The ICE 2005 database.

baseline algorithm and $\mathrm{EER} = 0.53\%$ for the modified algorithm with averaging) may be one of the best performance records that can be achieved at this point.

Fig. 16c shows the ROC curves of the proposed algorithms for the ICE 2005 database. NIST evaluates the performance of the ICE 2005 participants' algorithms by verification rate ($= 100\%$-FNMR) at $\mathrm{FMR} = 0.1\%$. Table 3 summarizes the ICE 2005 results reported by NIST [24]. It should be noted that the numbers in Table 3 are read out from the graphs in [24]. For a more detailed performance comparison, the reader is referred to the ROC curves shown in [24]. Note that we have participated in ICE 2005 (only Experiment 1) with our baseline algorithm and our result is labeled as "Tohoku" in the graphs in [24]. In contrast to the experimental results with CASIA version 1.0, the performance of the proposed baseline algorithm does not come up to those of other sate-of-the-art iris recognition algorithms. On the other hand, the modified algorithm with averaging shows comparable performance to other algorithms. The ICE 2005 participants are major players in iris recognition, so it can be said that the performance results listed in Table 3 are the world's highest records at present. This fact indicates that the phase-based iris recognition algorithm exhibits the top-level performance, despite its simplicity.

TABLE 1
Reported EERs from [4] (CASIA Version 1.0)

Method	EER [%]
Boles	8.13
Daugman	0.08
Ma	0.07
Tan	0.57
Wildes	1.76

TABLE 2
Reported EERs from [9] (CASIA Version 1.0)

Method	EER [%]
Daugman	0.70
Tan	0.51
Sun	0.86
Daugman + Sun	0.37
Tan + Sun	0.32
Daugman + Tan	0.49

TABLE 3
Reported Results of ICE 2005 [24]

Group	Verification rate at FMR=0.1% [%]	
	Experiment 1	Experiment 2
Carnegie Mellon University	99.6	99.1
Chinese Academy of Sciences	97.8	98.5
Indiana University, Purdue University, Indianapolis	79.9	76.6
Iritech	99.5	99.2
PELCO	96.8	96.6
SAGEM and Iridian Technologies Inc.	99.9	99.0
University of Cambridge	99.5	98.9
West Virginia University	97.8	96.8
Proposed (baseline)	93.2	87.5
Proposed (with averaging)	99.5	98.3

In the results of the ICE 2005 database, there is a significant performance difference between the baseline algorithm and the modified algorithm, while this difference was not observed in the experiments with the CASIA databases. This is mainly due to the fact that the quality of the iris images differs considerably between the CASIA databases and the ICE 2005 database. In the CASIA databases, the iris images are collected under well-controlled environments. On the other hand, the iris images in the ICE 2005 database are captured under less constrained conditions, so this database contains many challenging iris images with disturbances (for example, defocusing, blurring, and contact lens). For the ICE 2005 database, it is quite difficult to improve genuine matching scores because the image degradation causes serious differences between two iris images, even for genuine attempts. Thus, a practical approach to improving the recognition performance is to reduce the impostor matching score. As explained in Section 4.2, our modified algorithm contributes to reducing the impostor matching scores by decreasing the noise floor of the BLPOC function via spatial ensemble averaging. This is a major reason that the modified algorithm shows higher recognition performance than the baseline algorithm.

One of the difficult problems which is common to any database is the mislocalization of the iris. The preprocessing algorithm presented in Section 2 works well for most iris images used in our experiments, but, in some extreme cases (such as that shown in Fig. 17), the algorithm fails to segment the iris region. The mislocalization leads to the undesirable distortion of the normalized iris image, which reduces the height of correlation peak in genuine matching.

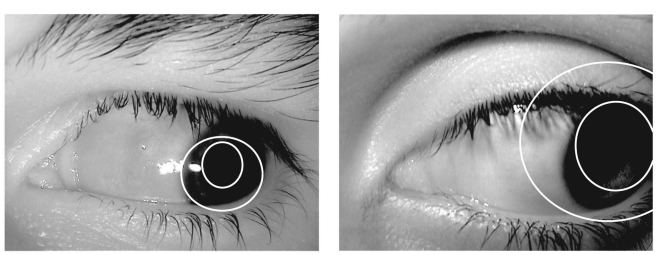

Fig. 17. Examples of mislocalization of the iris.

If the distortion is not significant, "*precise matching with scale correction*," as described in Section 4.1.4, is effective for recovering the peak value. At any rate, the preprocessing stage is important for achieving higher recognition performance. This fact is indirectly suggested by the performance analysis of 1D log-Gabor filter-based algorithms (shown in Fig. 16a), where improving the preprocessing algorithm gives a significant impact on the overall performance.

Consequently, the above-mentioned experimental trials clearly demonstrate the potential possibility of phase-based image matching for creating an efficient iris recognition system. The proposed baseline algorithm achieves highly accurate iris recognition with reduced computational complexity and the modified algorithm exhibits a significantly high performance, especially for degraded iris images.

6 Implementation-Oriented Iris Recognition Algorithm

This section discusses the major implementation issues of our algorithm. The proposed matching algorithm assumes the use of iris images directly in the system to achieve high recognition performance. In order to reduce the size of iris data and to prevent the visibility of individual iris images, we introduce here the idea of 2D FPC for representing iris information. The 2D FPC is particularly useful for implementing compact iris recognition devices using state-of-the-art DSP technology. By changing the degree of quantization in the 2D FPC, we can optimize the trade-off between the iris data size and recognition performance flexibly while avoiding the visibility of individual iris images.

The 2D FPC corresponds to the quantized version of the phase spectrum of a normalized iris image, which is essential for phase-based iris recognition. Instead of using iris images directly, the system registers 2D FPCs as biometric data. A major problem of this approach is that the 2D FPC does not contain amplitude spectrum and the actual iris image cannot be reconstructed from the 2D FPC. This causes problems in the "*effective region extraction*" stage and the "*displacement alignment*" stage in the flowchart shown in Fig. 1 since these two stages should be performed in the spatial image domain.

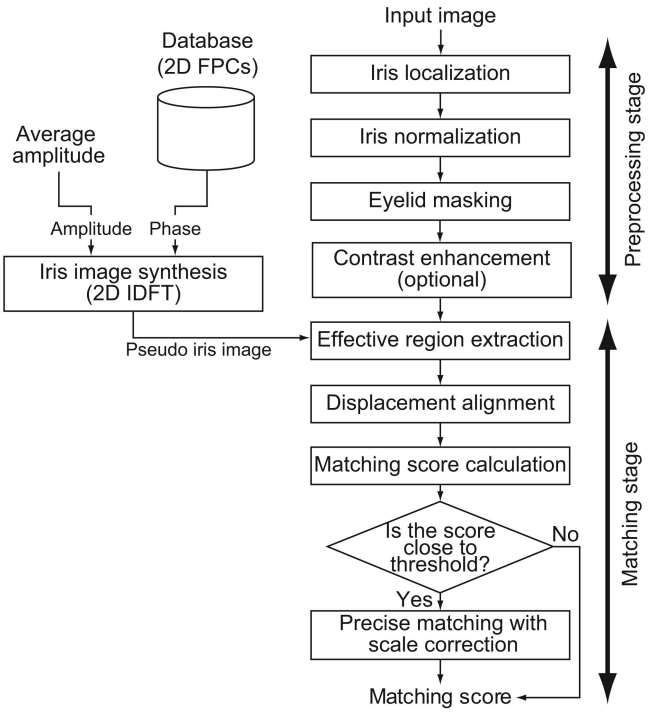

Fig. 18. Flow diagram of the proposed algorithm using 2D FPCs.

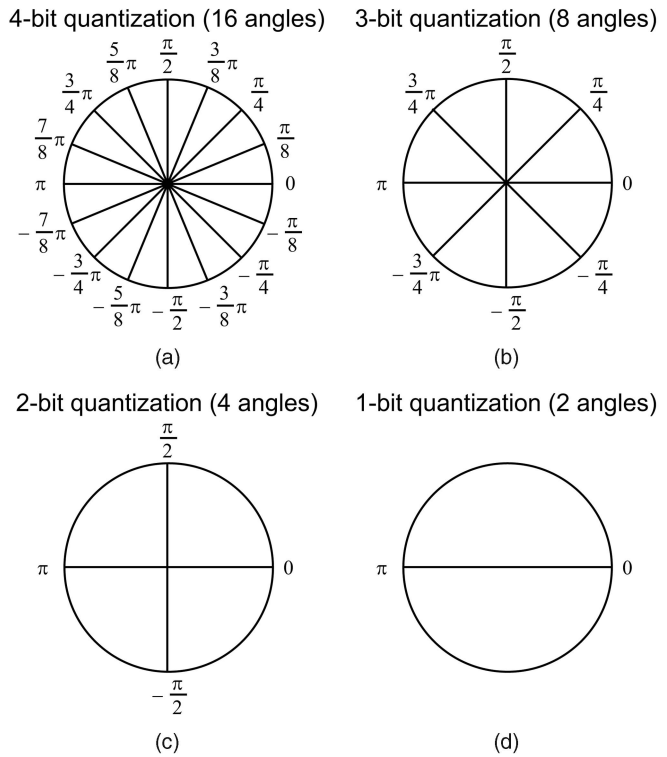

Fig. 19. Phase quantization. (a) Four-bit quantization. (b) Three-bit quantization. (c) Two-bit quantization. (d) One-bit quantization.

An idea for addressing this problem is to employ pseudo iris images synthesized from the corresponding 2D FPCs in the above two stages. The pseudo iris image preserves only the phase information of the original iris image. As for amplitude components, we use the average amplitude spectrum computed from the given database. Formally, the pseudo iris image $\tilde{f}$ of an iris image f is defined as the 2D IDFT of the pseudo complex spectrum $\tilde{F}$, whose amplitude $|\tilde{F}|$ is the average amplitude computed from many iris images and whose phase $\angle\tilde{F}$ is given by the 2D FPC of the iris image f.

Note here that we can use arbitrary chosen 2D amplitude spectra for $|\tilde{F}|$ to synthesize pseudo iris images. It is important to find an adequate amplitude spectrum which minimizes image distortion after the 2D IDFT. For example, the constant amplitude spectrum $|\tilde{F}| = 1$ is the simplest choice. However, our experimental observation shows that the use of the average amplitude spectrum exhibits much higher performance than the constant amplitude spectrum. Fig. 18 shows the flowchart of the iris recognition algorithm using 2D FPCs.

In general, the phase spectrum of a natural image has random values between $-\pi$ and π. Therefore, the quantization of phase components in the 2D FPC (Fig. 19) does not have a significant impact on the overall recognition performance. This property is particularly useful for reducing the iris data size while keeping a sufficient level of performance. In our original algorithm, the iris region is normalized into a rectangular image block of 256×128 pixels. Assuming 8-bit (256-level) quantization of pixel value, the total data size of an iris image becomes $256 \times 128 = 32$ Kbytes. On the other hand, the size of the 2D FPC with 4-bit quantization (Fig. 19a) can be reduced to 8 Kbytes by utilizing the symmetry of the phase spectrum. Similarly, the sizes of 2D FPCs with 3-bit, 2-bit, and 1-bit quantization are 6, 4, and 2 Kbytes, respectively (Figs. 19b, 19c, and 19d). Fig. 20 shows some examples of 2D FPCs with different degrees of quantization.

The performances of iris recognition algorithms using 2D FPCs are evaluated for the CASIA iris image databases

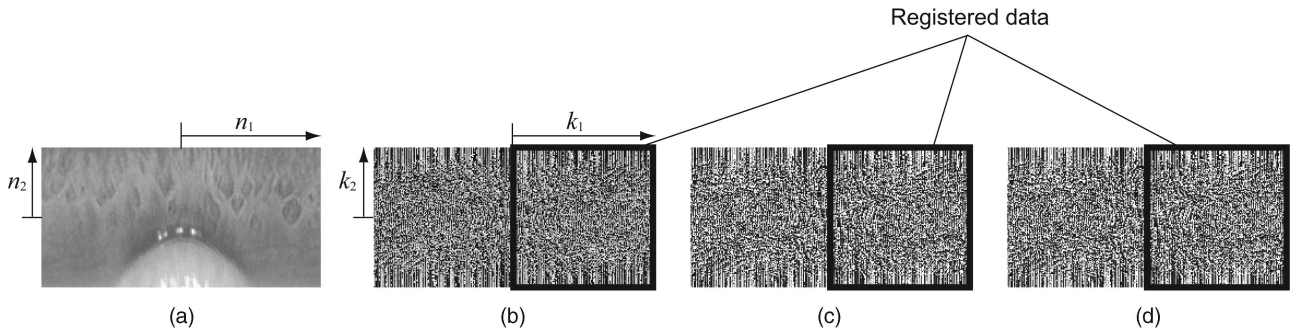

Fig. 20. 2D FPCs with different degrees of quantization. (a) Normalized iris image. (b) 2D FPC without quantization. (c) 2D FPC with 4-bit quantization. (d) 2D FPC with 2-bit quantization.

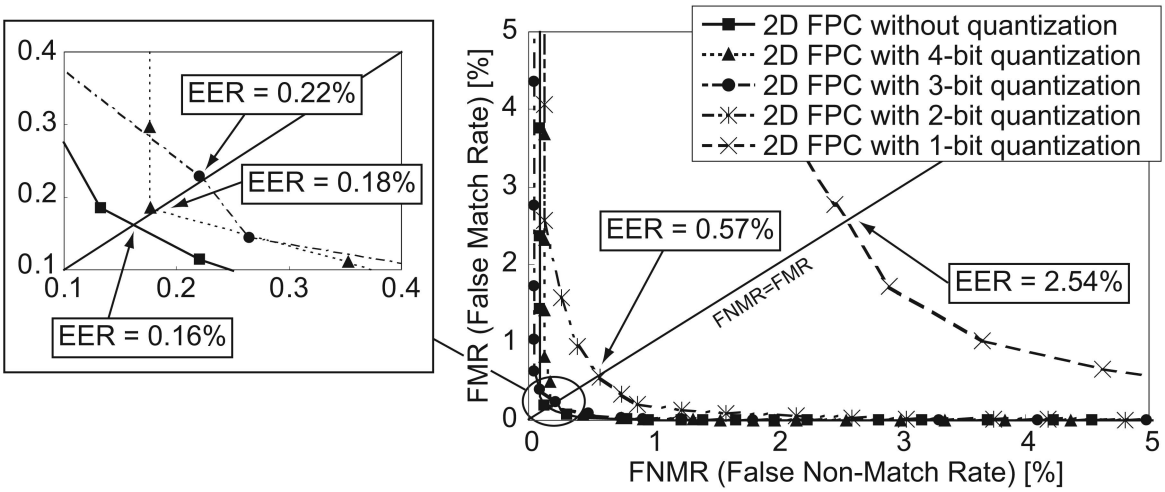

Fig. 21. ROC curves and EERs for CASIA version 1.0 using 2D FPCs with various levels of quantization.

TABLE 4
EERs for Different Types of Biometric Data Representation in the CASIA and ICE 2005 Databases

Type of registered biometric data	EER [%]		
	CASIA ver. 1.0	CASIA ver. 2.0	ICE 2005 (Experiment 1)
Normalized iris images	0.0032	0.53	0.33
2D FPCs with 4-bit quantization	0.18	0.61	0.54
2D FPCs with 2-bit quantization	0.57	0.77	0.83

(versions 1.0 and 2.0) and ICE 2005 database with various levels of phase quantization. The experimental conditions are the same as in Section 5. We use the baseline algorithm (described in Section 4.1) for CASIA version 1.0 and the modified algorithm (described in Section 4.2) for CASIA version 2.0 and ICE 2005. As an example, Fig. 21 shows the ROC curves for CASIA version 1.0 using 2D FPCs with different degrees of quantization. Table 4 summarizes the values of EER in the CASIA version 1.0, CASIA version 2.0, and ICE 2005 databases for three different types of biometric data representation: normalized iris images (used in the original algorithms), 2D FPCs with 4-bit, and 2D FPCs with 2-bit quantization. Although the 2D FPC-based algorithms exhibit higher EERs compared with the original algorithms described in Section 4, their performances with 4-bit quantization are still quite impressive.

These experimental results clearly demonstrate that 2D FPCs are particularly useful for implementing compact iris recognition devices using the DSP technology. We are now developing a very compact iris recognition device using 2D FPCs. On the other hand, the original phase-based iris recognition algorithm described in Section 4 is particularly suitable for implementing high-accuracy iris verification/identification systems, for which the recognition performance is a major concern.

7 Conclusion

Two major contributions of this paper can be summarized as follows:

- An effective approach for phase-based iris recognition is proposed in Section 4. Experimental performance evaluation using the CASIA iris image databases (versions 1.0 and 2.0) and the ICE 2005 database clearly demonstrates that the use of the Fourier phase spectra of iris images makes it possible to achieve highly accurate iris recognition with a simple matching algorithm.
- An implementation-oriented approach for phase-based iris recognition is proposed in Section 6. In order to reduce the size of registered iris data and to prevent the visibility of individual iris images, we introduce the idea of 2D FPC for representing iris information. The 2D FPC is particularly useful for implementing compact iris recognition devices using embedded microprocessors having DSP functionality. By changing the degree of phase quantization, we can optimize the trade-off between the iris data size and recognition performance in a highly flexible manner.

We believe that the phase-based image matching technique provides a unified framework for high-accuracy biometric authentication. We have already developed commercial fingerprint verification units using phase-based image matching [13], [14], [15], [16], [17]. In this paper, on the other hand, we have demonstrated that the same approach is also highly effective for iris recognition. Recently, we have also successfully applied the same technique to palmprint recognition [27]. Thus, the phase-based image matching provides a truly unified methodology for fingerprint, palmprint, and iris recognition, which will be particularly useful for developing multimodal biometric applications in the future.

Another important point to be noted is that the correlation-filter-based techniques for biometric authentication suggested by Vijaya Kumar et al., [8], [28], [29] are closely related to our approach. They propose potential

ideas for reducing the computational complexity in correlation-based pattern recognition [30]. These techniques seem to also be useful for our approach. Detailed investigations in this direction are left for our future study.

ACKNOWLEDGMENTS

Portions of the research in this paper use the CASIA iris image databases (versions 1.0 and 2.0) collected by the Institute of Automation, Chinese Academy of Sciences, and the ICE 2005 database collected by the National Institute of Standards and Technology.

REFERENCES

[1] J. Wayman, A. Jain, D. Maltoni, and D. Maio, *Biometric Systems.* Springer, 2005.
[2] A. Jain, R. Bolle, and S. Pankanti, *Biometrics: Personal Identification in a Networked Society.* Kluwer, 1999.
[3] J. Daugman, "High-Confidence Visual Recognition of Persons by a Test of Statistical Independence," *IEEE Trans. Pattern Analysis and Machine Intelligence,* vol. 15, no. 11, pp. 1148-1161, Nov. 1993.
[4] L. Ma, T. Tan, Y. Wang, and D. Zhang, "Efficient Iris Recognition by Characterizing Key Local Variations," *IEEE Trans. Image Processing,* vol. 13, no. 6, pp. 739-750, June 2004.
[5] W. Boles and B. Boashash, "A Human Identification Technique Using Images of the Iris and Wavelet Transform," *IEEE Trans. Signal Processing,* vol. 46, no. 4, pp. 1185-1188, Apr. 1998.
[6] C. Tisse, L. Martin, L. Torres, and M. Robert, "Person Identification Technique Using Human Iris Recognition," *Proc. 15th Int'l Conf. Vision Interface,* pp. 294-299, 2002.
[7] R. Wildes, "Iris Recognition: An Emerging Biometric Technology," *Proc. IEEE,* vol. 85, no. 9, pp. 1348-1363, Sept. 1997.
[8] B.V.K. Vijaya Kumar, C. Xie, and J. Thornton, "Iris Verification Using Correlation Filters," *Proc. Fourth Int'l Conf. Audio- and Video-Based Biometric Person Authentication,* pp. 697-705, 2003.
[9] Z. Sun, T. Tan, and X. Qiu, "Graph Matching Iris Image Blocks with Local Binary Pattern," *Advances in Biometrics,* vol. 3832, pp. 366-372, Jan. 2006.
[10] C.D. Kuglin and D.C. Hines, "The Phase Correlation Image Alignment Method," *Proc. Int'l Conf. Cybernetics and Soc. '75,* pp. 163-165, 1975.
[11] K. Takita, T. Aoki, Y. Sasaki, T. Higuchi, and K. Kobayashi, "High-Accuracy Subpixel Image Registration Based on Phase-Only Correlation," *IEICE Trans. Fundamentals,* vol. E86-A, no. 8, pp. 1925-1934, Aug. 2003.
[12] K. Takita, M.A. Muquit, T. Aoki, and T. Higuchi, "A Sub-Pixel Correspondence Search Technique for Computer Vision Applications," *IEICE Trans. Fundamentals,* vol. 87-A, no. 8, pp. 1913-1923, Aug. 2004.
[13] K. Ito, H. Nakajima, K. Kobayashi, T. Aoki, and T. Higuchi, "A Fingerprint Matching Algorithm Using Phase-Only Correlation," *IEICE Trans. Fundamentals,* vol. 87-A, no. 3, pp. 682-691, Mar. 2004.
[14] K. Ito, A. Morita, T. Aoki, T. Higuchi, H. Nakajima, and K. Kobayashi, "A Fingerprint Recognition Algorithm Using Phase-Based Image Matching for Low-Quality Fingerprints," *Proc. 12th IEEE Int'l Conf. Image Processing,* vol. 2, pp. 33-36, Sept. 2005.
[15] K. Ito, A. Morita, T. Aoki, T. Higuchi, H. Nakajima, and K. Kobayashi, "A Fingerprint Recognition Algorithm Combining Phase-Based Image Matching and Feature-Based Matching," *Advances in Biometrics,* vol. 3832, pp. 316-325, Jan. 2006.
[16] H. Nakajima, K. Kobayashi, M. Morikawa, A. Katsumata, K. Ito, T. Aoki, and T. Higuchi, "Fast and Robust Fingerprint Identification Algorithm and Its Application to Residential Access Controller," *Advances in Biometrics,* vol. 3832, pp. 326-333, Jan. 2006.
[17] Products Using Phase-Based Image Matching, Graduate School of Information Sciences, Tohoku Univ., http://www.aoki.ecei.tohoku.ac.jp/research/poc.html, 2008.
[18] K. Miyazawa, K. Ito, T. Aoki, K. Kobayashi, and H. Nakajima, "An Efficient Iris Recognition Algorithm Using Phase-Based Image Matching," *Proc. 12th IEEE Int'l Conf. Image Processing,* vol. 2, pp. 49-52, Sept. 2005.
[19] K. Miyazawa, K. Ito, T. Aoki, K. Kobayashi, and H. Nakajima, "A Phase-Based Iris Recognition Algorithm," *Advances in Biometrics,* vol. 3832, pp. 356-365, Jan. 2006.
[20] CASIA Iris Image Database, Inst. Automation, Chinese Academy of Sciences, http://www.sinobiometrics.com/, 2008.
[21] Iris Challenge Evaluation (ICE), Nat'l Inst. Standards and Technology, http://iris.nist.gov/ice/, 2008.
[22] R.C. Gonzalez and R.E. Woods, *Digital Image Processing,* second ed. Prentice Hall, 2002.
[23] L. Masek and P. Kovesi, "Matlab Source Code for a Biometric Identification System Based on Iris Patterns," School of Computer Science and Software Eng., Univ. of Western Australia, http://people.csse.uwa.edu.au/pk/studentprojects/libor/, 2003.
[24] ICE 2005 Results, Nat'l Inst. Standards and Technology, http://iris.nist.gov/ICE/ICE_2005_Results_30March2006.pdf, 2008.
[25] B. Efron, "Bootstrap Methods: Another Look at the Jackknife," *Annals of Statistics,* vol. 7, no. 1, pp. 1-26, 1979.
[26] R.M. Bolle, N.K. Ratha, and S. Pankanti, "Error Analysis of Pattern Recognition Systems: The Subsets Bootstrap," *Computer Vision and Image Understanding,* vol. 93, no. 1, pp. 1-33, Jan. 2004.
[27] K. Ito, T. Aoki, H. Nakajima, K. Kobayashi, and T. Higuchi, "A Palmprint Recognition Algorithm Using Phase-Based Image Matching," *Proc. 13th IEEE Int'l Conf. Image Processing,* pp. 2669-2672, Oct. 2006.
[28] B.V.K. Vijaya Kumar, M. Savvides, K. Venkataramani, and C. Xie, "Spatial Frequency Domain Image Processing for Biometric Recognition," *Proc. Ninth IEEE Int'l Conf. Image Processing,* vol. 1, pp. 53-56, 2002.
[29] K. Venkataramani and B.V.K. Vijaya Kumar, "Performance of Composite Correlation Filters for Fingerprint Verification," *Optical Eng.,* vol. 43, pp. 1820-1827, Aug. 2004.
[30] B.V.K. Vijaya Kumar, A. Mahalanobis, and R. Juday, *Correlation Pattern Recognition.* Cambridge Univ. Press, 2005.

Kazuyuki Miyazawa received the BE degree in information engineering and the MS degree in information sciences from Tohoku University, Sendai, Japan, in 2005 and 2007, respectively. He is currently working toward the PhD degree and is a research fellow of the Japan Society for the Promotion of Science. His research interests include signal and image processing and biometric authentication. He is a student member of the IEEE.

Koichi Ito received the BE degree in electronic engineering and the MS and PhD degrees in information sciences from Tohoku University, Sendai, Japan, in 2000, 2002, and 2005, respectively. He is currently an assistant professor in the Graduate School of Information Sciences at Tohoku University. From 2004 to 2005, he was a research fellow of the Japan Society for the Promotion of Science. His research interests include signal and image processing, and biometric authentication. He is a member of the IEEE.

Takafumi Aoki received the BE, ME, and DE degrees in electronic engineering from Tohoku University, Sendai, Japan, in 1988, 1990, and 1992, respectively. He is currently a professor in the Graduate School of Information Sciences at Tohoku University. From 1997 to 1999, he was with the PRESTO Project, Japan Science and Technology Corp. (JST). His research interests include the theoretical aspects of computation, VLSI systems, multiple-valued logic, digital signal processing, image sensing, computer vision, biometric authentication, and secure embedded systems. He received the Outstanding Paper Award from the 20th IEEE International Symposium on Multiple-Valued Logic (ISMVL '90), ISMVL '00, ISMVL '01, and ISMVL '06, the Outstanding Transaction Paper Awards from the IEICE of Japan in 1989 and 1997, the IEE Ambrose Fleming Premium Award in 1994, the IEICE Inose Award in 1997, the IEE Mountbatten Premium Award in 1999, and the Best Paper Awards from the 1999 IEEE International Symposium on Intelligent Signal Processing and Communication Systems (ISPACS) and the 14th Workshop on Synthesis And System Integration of Mixed Information technologies (SASIMI '07). He is a member of the IEEE and the IEEE Computer Society.

Koji Kobayashi received the BE and ME degrees in electronic engineering from Tohoku University, Sendai, Japan, in 1976, and 1978, respectively. He is currently the director of the Residential Building Department, Building Systems Co., Yamatake Corp., Tokyo. His research interests include real-time automation system architecture, network communication protocol LSI, biometric image processing, CMOS image sensor, and 3D sensing. He is a member of the IEEE.

Hiroshi Nakajima received the BE degree in electronic engineering from Tohoku University, Sendai, Japan, in 1990. He is currently the assistant manager of the Development Department 2, Building Systems Co., Yamatake Corp., Fujisawa, Japan. His research interests include biometric image processing and 3D sensing and processing.